Original Article

MOLECULAR METABOLISM

Functional loss of inactive rhomboid-like protein 2 mitigates obesity by suppressing pro-inflammatory macrophage activation-triggered adipose inflammation

Minxuan Xu [1,2,3,*,5], Chenxu Ge [1,2,3,5], Yuting Qin [4,5], Deshuai Lou [1,2], Qiang Li [1,2], Jing Feng [1,2], Yekuan Wu [1,2], Linfeng Hu [1,2], Bochu Wang [3,***], Jun Tan [1,2,**]

ABSTRACT

Objective: Chronic inflammation of adipose tissues contributes to obesity-triggered insulin resistance. Unfortunately, the potential molecular mechanisms regarding obesity-associated systemic inflammation and metabolic disorder remain complicated. Here, we report that inactive rhomboid-like protein 2 (iRhom2) was increased in overweight mice with adipose inflammation.

Methods: Mice with deletion of iRhom2 on a C57BL/6J background, mice without deletion of this gene (controls), and mice with deficiency of iRhom2 only in myeloid cells were fed a standard chow diet (SCD) or a high-fat diet (HFD; 60% fat calories). Then the adipose tissues or bone marrow cells were isolated for the further detection.

Results: After 16 weeks on a high-fat diet (HFD), obesity, chronic inflammation in adipose tissues, and insulin resistance were markedly mitigated in iRhom2 knockout (iRhom2 KO) mice, whereas these parameters were exaggerated in iRhom2 overactivated mice. The adverse influences of iRhom2 on adipose inflammation and associated pathologies were determined in *db*/*db* mice. We further demonstrated that, in response to an HFD, iRhom2 KO mice and mice with deletion only in the myeloid cells showed less severe adipose inflammation and insulin resistance than control groups. Conversely, transplantation of bone marrow cells from normal mice to iRhom2 KO mice unleashed severe systemic inflammation and metabolic dysfunction after HFD ingestion.

Conclusion: We identified iRhom2 as a key regulator that promotes obesity-associated metabolic disorders. Loss of iRhom2 from macrophages in adipose tissues may indirectly restrain inflammation and insulin resistance via blocking crosslinks between macrophages and adipocytes. Hence, iRhom2 may be a therapeutic target for obesity-induced metabolic dysfunction.

Keywords iRhom2; Adipose inflammation; Insulin resistance; Dyslipidemia

1. INTRODUCTION

Obesity is a globally increasing public health threat that can cause metabolic diseases, such as cardiac-cerebral vascular disease, cognitive dysfunction, type II diabetes, and cancer. A prolonged high-fat diet (HFD) induces sterile inflammation in white adipose tissue (WAT), which is an important locus for energy homeostasis of triglycerides (TGs) and for homeostatic- and nutrition-induced production/secretion of hormones and cytokines that exhibits a critical role in obesity-triggered systemic insulin resistance and its associated metabolic dysfunction [1–3]. Unfortunately, the molecular mechanisms by which nutritive obesity initiates systemic inflammation and metabolic disorder are still not fully understood.

Accumulating evidence has recently indicated an important role for innate immunity in crosstalk with the progression of obesity [4]. As one of the most essential cells in adipose tissue-associated innate

[1]Chongqing Key Laboratory of Medicinal Resources in the Three Gorges Reservoir Region, School of Biological and Chemical Engineering, Chongqing University of Education, Chongqing, 400067, PR China [2]Research Center of Brain Intellectual Promotion and Development for Children Aged 0-6 Years, Chongqing University of Education, Chongqing, 400067, PR China [3]Key Laboratory of Biorheological Science and Technology (Chongqing University), Ministry of Education, College of Bioengineering, Chongqing University, Chongqing, 400030, PR China [4]School of Medicine and Pharmacy, Ocean University of China, Qingdao, 266100, PR China

[5] These authors contributed equally to this work.

*Corresponding author. Chongqing Key Laboratory of Medicinal Resources in the Three Gorges Reservoir Region, School of Biological and Chemical Engineering, Chongqing University of Education, Chongqing, 400067, PR China. E-mail: minxuanxu@foxmail.com (M. Xu).

***Corresponding author. E-mail: wangbc2000@126.com (B. Wang).

**Corresponding author. Research Center of Brain Intellectual Promotion and Development for Children Aged 0-6 Years, Chongqing University of Education, Chongqing, 400067, PR China. E-mail: tanjun@cque.edu.cn (J. Tan).

Received April 16, 2019 • Revision received December 23, 2019 • Accepted January 14, 2020 • Available online 22 January 2020

https://doi.org/10.1016/j.molmet.2020.01.008

Abbreviations

BAT	brown adipose tissue
PPARγ	peroxisome proliferator-activated receptorγ
iRhom2	inactive rhomboid-like protein 2
IL-18	interleukin 18
WAT	white adipose tissue
SREBP-1c	sterol regulatory element-binding protein 1c
TG	triacylglycerol
FATP1	fatty acid transport protein 1
FABP1	fatty acid-binding protein 1
SCD1	stearoyl-CoA desaturase
ACCα	acetyl CoA carboxylase α
ABCG1	ATP-binding cassette sub-family G member 1
CYP7A1	cholesterol 7α-hydroxylase
PDK4	pyruvate dehydrogenase kinase 4
PPARα	peroxisome proliferator-activated receptor α
CPT-1α	carnitine palmitoyltransferase 1α
ACOX-1	acyl-coenzyme A oxidase 1
LCAD	long-chain acyl-CoA dehydrogenases
MCAD	medium-chain acyl-CoA dehydrogenase
UCP2	uncoupling protein 2
SCD	standard chow diet
HFD	high-fat diet

immunity, adipose tissue macrophages have received attention due to their core function in pro-inflammatory activation and their connection to metabolic dysfunction [5,6]. Nutritive obesity significantly promotes increased macrophage infiltration in adipose tissue, induces macrophage overactivation, and upregulates the generation of pro-inflammatory cytokines and chemokines (such as tumor necrosis factor-α [TNF-α] and monocyte chemoattractant protein-1 [MCP-1]; [7,8]). Thus, a series of regulators, including nuclear factor κB (NF-κB), transforming growth factor-activated kinase-1 (TAK1), and insulin receptor substract-1 (IRS-1), have been confirmed to participate in the inflammatory responses of macrophages and in the development of insulin resistance, which then provides crosstalk with adipocytes to protect against or promote adipose inflammation-associated obesity. These previous studies highlighted the importance of the innate immunity system, especially in terms of the role of macrophages in obesity [9–11]. However, it is still largely unknown as to how these factors in the innate immunity system markedly regulate metabolic balance, inflammation, and its relationship in the process of obesity identification.

Inactive rhomboid protein 2 (iRhom2), also known as Rhbdf2, is an inactive member of the rhomboid intramembrane-proteinase family of serine proteases and has been shown to play crucial roles in regulating protein degradation, trafficking regulation, and inflammatory response [12–14]. With metabolic disorder or changes in innate immunity, the expression of iRhom2 in macrophages is significantly upregulated and promotes TNF-α production by trafficking of the TNF-α-converting enzyme (ADAM17). This process leads to the activation of downstream cascades that involve tumor necrosis factor receptor 1/2 (TNFR1/2), TAK1, NF-κB, and numerous cytokines or chemokines to accelerate inflammatory response and macrophage infiltration [15–17]. These findings have contributed to several recent conclusions regarding how iRhom2 regulates immunoreactions stimulated by viral infection, arthritis, and lupus nephritis [14,18,19]. Of note, our preliminary study also indicated that iRhom2 plays an essential role in early kidney injury by regulating inflammation and oxidative stress. Additionally, the overexpression of iRhom2, as a promoter in inflammatory responses, contributes to acute hepatic injury and the occurrence of systemic metabolism disorder [20]. However, the correlation of iRhom2 to nutritive obesity-associated adipose inflammation and insulin resistance has not previously been investigated. Also, TNF-α-dependent activation and generation by iRhom2 is only exhibited in immune cells [21]. Given these findings, it is crucial to elucidate the precise role of iRhom2 in the occurrence and development of obesity-associated adipose inflammation and insulin resistance. The present study highlights the harmful role of iRhom2 in obesity, the effects of which may be mediated by promoting macrophage activation of adipose and systemic inflammation.

2. MATERIALS AND METHODS

2.1. Study approval and ethics statement

All of the research procedures associated with mice were approved by the Institutional Animal Care and Use Committee at the Chongqing Key Laboratory of Medicinal Resources in the Three Gorges Reservoir Region, School of Biological and Chemical Engineering, Chongqing University of Education, and were conducted in accordance with the Guide for the Care and Use of Laboratory Animals issued by the National Institutes of Health in 1996. The protocols used in this study were in accordance with the Regulations of Experimental Animal Administration issued by the Ministry of Science and Technology of the People's Republic of China (http://www.most.gov.cn).

2.2. Animal administration and experiment design

Inactive rhomboid-like protein 2 (iRhom2) deletion mice with a C57BL/6 background were used in this study as described previously [17]. Wild-type (WT) C57BL/6N mice were purchased from Beijing Vital River Laboratory Animal Technology Co., Ltd. (Beijing, China). Prior to all of the experiments, the mice were allowed to adapt to the environment for 7 days. The mice were maintained in a constant temperature (controlled by GREE air conditioner), humidity, and pathogen-free controlled environment (25 °C ± 2 °C, 50%–60%) with a standard 12 h light/12 h dark cycle and abundant food and water (pathogen-free) in their cages.

Model 1#. Male WT mice at the age of 6–8 weeks or *db/db* mice were accordingly produced by feeding a high-fat diet (HFD) fodder (20% kcal protein, 60 kcal% fat, and 20% kcal carbohydrate, Cat#: D12492; Research Diets, New Brunswick, NJ, USA) for 16 weeks until the experimental mice were sacrificed for further study. In addition, the mice that were fed a standard chow diet (20% kcal protein, 10 kcal% fat and, 70% kcal carbohydrate, Cat#: D12450H; Research Diets) as a control group (SCD). After the feeding period, the mice were collected to investigate white adipose tissue signaling items downstream of iRhom2 associated with diet-induced adipose inflammation.

Model 2#. Male iRhom2 knockout (KO) mice and WT mice at the age of 6–8 weeks were fed an HFD diet for 16 weeks to detect the changes in iRhom2 expression, adipose inflammation, and insulin resistance. Age-matched male KO mice and WT mice were separately fed SCD fodder for 16 weeks and treated as controls.

Model 3#. Male WT mice at the age of 6–8 weeks were fed an HFD diet for the first 4 weeks. Then an adenovirus-associated virus 8

(AAV8) delivery system was used to overexpress iRhom2 in the adipose tissue. Briefly, the opening reading frame (ORF) encoding iRhom2 without a stop codon was cloned into an pAAV-CMV vector to generate pAAV-CMV-Rhbdf2-2 A-EGFP-3FLAG-CW3SL. Accordingly, the mice were injected with vector via the tail vein with 100 μl of virus containing 2×10^{11} vg of AAV8 vectors and fed an HFD for an additional 12 weeks. The empty vector based on pAAV-CMV was used as a control.

Model 4#. Male WT mice at the age of 6–8 weeks were lethally irradiated and then subjected to bone marrow transplantation (BMT) surgery with bone marrow cells isolated from the iRhom2 KO mice and WT mice and treated as WTBM → WT/HFD and KOBM → WT/HFD mice, respectively, as described previously [26,27]. After recovery for 4 weeks, the mice were fed an HFD for 16 weeks as described in model #2.

Model 5#. Male iRhom2 KO mice at the age of 6–8 weeks were lethally irradiated and then subjected to bone marrow transplantation (BMT) surgery with bone marrow cells collected from the iRhom2 KO mice and WT mice and treated as KOBM → KO/HFD and WTBM → KO/HFD mice, respectively. After recovery for 4 weeks, the mice were fed an HFD for 16 weeks as described in model #2.

During the feeding period, fasting blood glucose and insulin, body weight, food, and water intake were recorded every 4 weeks or every week in the model #2 mice. The body weight and body composition associated BMT mice were examined at the first week and last week during the experimental period. The eye blood serum was harvested from all of the mice and stored at −20 °C. Epididymal white adipose tissues (eWAT) and inguinal white adipose tissues (iWAT) were also carefully isolated and stored at −80 °C for corresponding tissue analysis treatment fluid.

2.3. Body composition, glucose, and insulin tolerance detection

The mice body composition including lean mass, fat mass, relative percent of fat, and relative bone mineral density were examined using Dual-Energy X-ray absorptiometry (DEXA) (GE Medical Systems, China). For the glucose tolerance test (GTT) and insulin tolerance test (ITT) detection, all of the mice were fasted for 8 h to confirm the correction of the physiological response. The mice were intraperitoneally injected with glucose (2 g/kg body weight) (Cat#: D810588, Macklin Inc., Shanghai, China). Then the concentrations of blood glucose of the tail venous blood at 0 min, 15 min, 30 min, 60 min, and 120 min after glucose treatment were examined using commercial blood glucose test strips (ACCU-CHEK, Roche Diabetes Care GmbH, Shanghai, China). To detect insulin resistance, the mice were intraperitoneally injected with insulin (1 U/kg body weight, Sigma Aldrich). The GTT and ITT protocol were used in accordance with our previous research [40]. Subsequently, blood samples were collected from the tail vein at 0 min, 15 min, 30 min, 60 min, and 120 min post-injection to measure the glucose levels. Homeostasis model assessment (HOMA)-IR was calculated from the fasting levels of the glucose and insulin in the serum, respectively.

2.4. Histological examination

The fat tissue samples from each group of mice were fixed with 4% paraformaldehyde, embedded in paraffin, and sectioned transversely. Adipose or liver tissues were subjected to hematoxylin and eosin (H&E) or Oil Red O staining to visualize the patterns of lipid accumulation and the impaired status of the tissues. Briefly, the mice liver and white adipose tissues were fixed with 4% paraformaldehyde (Cat#: P1110, Solarbio Life Sciences, Beijing, China), embedded in paraffin (Cat#: P100928, Aladdin, Shanghai, China), and sectioned transversely. Thin sections were stained with H&E (Hematoxylin and Eosin Staining Kit, Yeasen, Shanghai, China) according to standard histopathological processes. All of the sections were detected by 3 histologists without knowledge of the treatment procedure. To visualize the lipid accumulation, the tissues were frozen in Tissue-Tek OCT (Tissue-Tek, Sakura Finetek, Torrance, CA, USA) and the sections were then stained with an Oil Red O Staining Kit (Cat#: G1260, Solarbio Life Sciences, Beijing, China) for 10 min. After rinsing with 60% isopropyl alcohol (Cat#: I811925, AR, Macklin Inc., Shanghai, China), the tissue sections were re-stained with hematoxylin. For the immunohistochemistry assay, embedded sections were deparaffinized before administration with primary antibodies at 4 °C overnight. The tissues were subjected to immunohistochemical (IHC) staining to measure the F4/80 (Abcam, ab100790, dilution 1:300) expression. All of the histological procedures were conducted in accordance with the standard procedures as indicated in the reagent specifications. All of the images were captured using an optical microscope (Olympus, Japan).

2.5. Adipose cell isolation, adipocyte sizes, and number detection

Purified adipose cells of epididymal WAT (eWAT) and inguinal WAT (iWAT) and number detection were conducted according to a described previously protocol [41,43]. In brief, the corresponding fat tissues were harvested and minced in a sterile 150 mm dish with abundant Hank's balanced salt solution (HBSS) using sterile scissors in a laminar flow hood. Then the tissues were digested with sterile enzyme solution (2 mg of collagenase in 2 ml of isolation buffer containing 0.123 M NaCl, 5 mM KCl, 1.3 mM $CaCl_2$, 5 mM glucose, 100 mM Hepes, and 4% BSA) at 37 °C for 45 min. After enzymatic cell dispersal, the tissues were filtered through a sterile 1000 μm plastic mesh in a sterile funnel into a sterile 50 ml centrifuge tube. The filtrate was centrifuged for 10 min at 186×*g*. The underlying pellets (containing preadipocytes, fibroblasts, and erythrocytes) and media were removed from the laminar flow hood. To detect the stromal vascular fraction, the underlying pellets were transferred to a tissue culture flask with serum-containing medium. The remaining fat layer was re-suspended in 20 ml of HBSS and centrifuged for 10 min at 186×*g*. This step was repeated two additional times. The upper cells (adipocytes) and underlying cells (stromal vascular cells) were collected for the further experiments.

The average cell diameter was examined using ImageJ software from the National Institutes of Health (NIH). The total adipose cell numbers were determined by counting the cells on the H&E sections from at least 3 fields per mouse. The size of the cells was approximated assuming cubic packing as previously indicated [41].

2.6. F4/80-positive macrophage collection from adipose tissues

The F4/80-positive (F4/80+) macrophages in the adipose tissues were collected according to previous studies with modifications [7,42] and the manufacturer's instructions. The F4/80 ± macrophages (MΦ) from the stromal vascular fraction (SVF) of the adipose tissues were isolated and purified using PE magnetic particle separation as indicated in the manufacturer's specifications. In brief, 2×10^7 SVF cells were re-suspended in 120 μl Hank's buffer (Solarbio, Beijing, China), stained with 15 μl of mouse PE-conjugated F4/80 mAbs (Cat#: FAB5580P-100UG, R&D Systems), and co-incubated with 30 μl of anti-PE magnetic beads for 20 min. The washed cells were re-suspended in 1 ml of Hank's buffer and then subjected to XS separation (MACS, Miltenyi Biotec). The positive MΦ cells were eluted and harvested for further experiments.

2.7. Real-time quantitative PCR

TRIzol (Cat#:15596026, Invitrogen, Thermo-Fisher Scientific, Waltham, MA, USA) was used to collect the total RNA extraction from the cells and adipose tissues. In brief, 1 μg of total RNA samples were reverse transcribed using an M-MLV-RT system (Invitrogen, Shanghai, China) at 42 °C for 1 h and terminated by deactivation of the enzymes at 70 °C for 10 min. PCR was conducted using SYBR Green (Bio-Rad) in an ABI PRISM 7900HT detection system (Applied Biosystems, Foster City, CA, USA). Pre-denatured amplification products were processed at 94 °C for 55s, followed by 45 cycles at 95 °C for 30 s, 57 °C for 30 s, and 73 °C for 30s, followed by 95 °C for 10 s, 65 °C for 45 s, and 40 °C for 60 s. The fold induction values were calculated according the $2^{-\Delta\Delta Ct}$ expression, where $^{\Delta}Ct$ represents the differences in the cycle threshold numbers between the target genes and GAPDH and $^{\Delta\Delta}Ct$ represents the relative change in the differences between the control and treatment groups. The RT-PCR primer sequences were produced by Sangon Biotech (Shanghai) Co., Ltd., and are shown in Table S1.

2.8. Immunoblotting assay

For western blotting examination, the cells and tissues were homogenized in 10% (wt/vol) RIPA lysis buffer (pH 8.0, 1 mM EDTA, 50 μg/ml aprotinin, 25 mM Tris-HCl, 5 μg/ml leupeptin, 1 mM Pefabloc SC, 4 mM benzamidine, and 5 μg/ml soybean trypsin inhibitor) to yield a homogenate. The final liquid supernatants were then harvested via centrifugation at 13500 rpm and 4 °C for 30 min. The protein concentration was measured using a Pierce Rapid Gold BCA Protein Assay Kit (Thermo-Fisher) with bovine serum albumin as a standard. The total protein was extracted for western blotting. Equal amounts of the total protein of the tissues were subjected to 10%—12% SDS-PAGE and then transferred to a 0.45 μM PVDF membrane (Millipore, Burlington, MA, USA) followed by immunoblotting using the primary antibodies. The primary antibodies used in this study included anti-GAPDH (Abcam, ab8245, dilution 1:5000), anti-tubulin (Abcam, ab7291, dilution 1:5000), anti-p-IRS-1 (Y608) (Millipore, dilution 1:1000), IRS-1 (Abcam, ab52167, dilution 1:1000), p-AKT (CST, 4060, dilution 1:1000), AKT (CST, 4691, dilution 1:1000), p-GSK3β (CST, 9322, dilution 1:1000), GSK3β (CST, 12456, dilution 1:1000), FOXO1 (CST, 2880, dilution 1:1000), p-FOXO1 (Abcam, ab131339, dilution 1:1000), PEPCK (Santa-Cruz, sc-271029, dilution 1:1000), anti-;NF-κB (Abcam, ab16502, dilution 1:1000), anti-p-NF-κB (Abcam, ab86299, dilution 1:1000), anti-Rhbdf2 (Biobyt, orb386934, dilution 1:1000), anti-TNF-α (CST, 3707, dilution 1:1000), anti-TNFR1 (Abcam, ab19139, dilution 1:1000), anti-TNFR2 (Abcam, ab109322, dilution 1:1000), anti-IκBα (Abcam, ab32518, dilution 1:1000), anti-p-IκBα (CST, 9246, dilution 1:1000), anti-TAK1 (Abcam, ab109526, dilution 1:1000), and anti-p-TAK1 (CST, 9339, dilution 1:1000). The membranes were blocked with 5% skim milk (Difco Skim Milk, BD Biosciences, Franklin Lakes, NJ, USA) in 1 × TBS buffer (Cat#: T1080, Solarbio, Beijing, China) containing 0.1% Tween-20 (1247ML100, BioFroxx, Germany) (TBST) for 1 h and incubated with the primary antibodies in a refrigerator overnight at 4 °C. The membranes were rinsed in 1 × TBST and incubated with HRP-conjugated anti-rabbit or anti-mouse secondary antibodies (Abcam) for 1—2 h at room temperature (25 °C). The bands were visualized using Enhanced New Super ECL Western Blotting Substrate (KeyGEN Biotech, China) and exposed to X-ray film (Eastman Kodak Company, Rochester, NY, USA). The corresponding protein expression was determined as the gray value (Version 1.52 g, Mac OS X, ImageJ, National Institutes of Health, Bethesda, MD, USA), standardized to housekeeping genes (GAPDH), and expressed as the fold change.

2.9. Measurement of the cytokines and chemokines produced

The cytokines and chemokines of the mice were detected using corresponding commercial ELISA kits. TNF-α (Cat#: MTA00B), IL-1β (Cat#: MLB00C), IL-6 (Cat#: M6000B), IL-18 (Cat#: DY122-05), MCP-1 (Cat#: SMJE00B), CCL1 (Cat#: DY845), IL-17 (Cat#: SM1700), IL-2 (Cat#: SM2000), IL-10 (Cat#: SM1000B), IL-5 (Cat#: SM5000), MIP-2 (Cat#: SMM200), MIP-3β (Cat#: DY440), MDC (Cat#: MCC220), CX3CL1 (Cat#: MCX310), CXCL10 (Cat#: DY466-05), and CXCL12 (Cat#: DY460) ELISA kits were purchased from R&D Systems (Shanghai, China) and used according to the product specifications. An MCP-3 (Cat#: BMS6006INST) ELISA kit was acquired from Invitrogen. A GCP-2 (Cat#: ab100719) kit was obtained from Abcam. An HMGB1 ELISA kit (Cat#: 326054329) was purchased from Shino-Test Corporation (Kanagawa, Japan). A procalcitonin ELISA kit (Cat#: EF014005) was obtained from Life Sciences. All the corresponding serum was carefully stored at −80 °C in a refrigerator until it was used.

2.10. Statistical analysis

The data were expressed as mean ± standard error of the mean (SEM). Comparisons between all of the groups were analyzed via one-way ANOVA followed by Dunnett's multiple comparisons test or Student's unpaired 2-tailed *t*-test. GraphPad Prism Software (version 7.0 for Mac OS X Snow Leopard; GraphPad Software, Inc., San Diego, CA, USA) was used for the analysis. A p-value less than 0.05 was considered significant.

3. RESULTS

3.1. iRhom2 expression increased in the adipose tissues and was involved in adipose inflammation and macrophage activation

To assess the correlation of iRhom2 with adipose inflammation, we investigated iRhom2 activity in adipose tissues isolated from obese mice. The expression of iRhom2 was significantly upregulated in the epididymal WAT (eWAT), inguinal WAT (iWAT), and purified adipocytes derived from the iWAT or eWAT of HFD-stimulated obese mice or *db/db* mice, which was associated with increased TNF-receptor 1 and 2. Consistent with this finding, in response to iRhom2 activation, the obese mice demonstrated increased phosphorylation of NF-κB and pro-inflammatory cytokines of TNF-α in the downstream iRhom2 pathway compared to the SCD groups (Figure 1 A-D and Figure 1A—C). The adipose tissues contained not only adipose cells, but also macrophages and other types of cells. Hence, we further detected changes in the iRhom2 expression in the isolated F4/80-positive macrophages (MΦs) and stromal vascular fraction cells (SVFs) from the adipose tissues. HFD ingestion significantly elevated the iRhom2 expression levels in the MΦs derived from the iWAT and eWAT and induced the activation of iRhom2 downstream-signaling targets, including phosphorylation of NF-κB and TNF-α secretion (Figures S1D and E). Concurrent with the upregulation of iRhom2 activity in the MΦs, obesity markedly elevated iRhom2/TNF-α/p-NF-κB signaling in the SVFs collected from fat tissues (Figures S1F and G). These findings suggest that activation of iRhom2 and its downstream events may contribute to HFD-triggered inflammatory responses.

3.2. iRhom2 deletion protects against high-fat diet-induced obesity and insulin resistance

Many studies have indicated that the overexpression of iRhom2 and its downstream events may participate in the development of metabolic syndrome [17,22]. We examined the role of iRhom2 in HFD-induced metabolic changes. The body weights of the mice were dramatically increased in both the HFD-fed WT and iRhom2 knockout (KO) mice

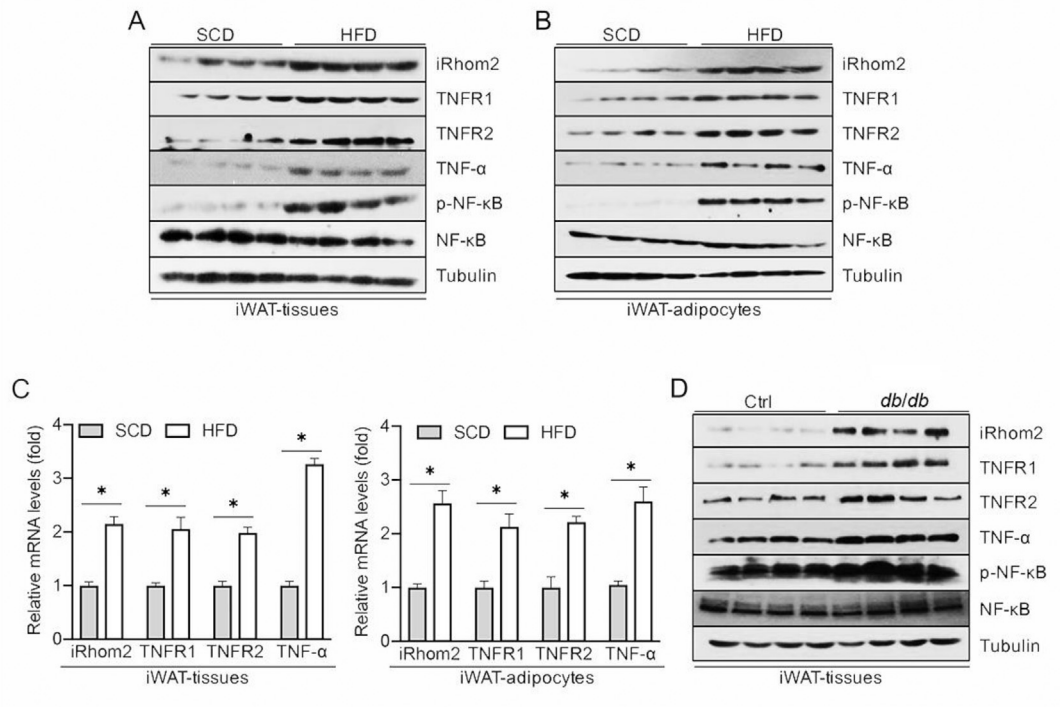

Figure 1: iRhom2 increases in adipose tissues and promotes adipose inflammation in obese mice. (A) Western blotting for the expression of iRhom2, TNFR1/2, TNF-α, and phosphorylated NF-κB in iWAT harvested from standard chow diet and high-fat diet-fed C57BL/6N mice. (B) Western blotting of isolated adipocytes in iWAT of SCD and HFD-fed C57BL/6N mice. (C) qPCR expression changes in iRhom2, TNFR1/2, and TNF-α from iWAT or adipocytes in SCD and HFD-fed C57BL/6N mice; $n = 6$. (D) Western blotting of iWAT from *db/db* and corresponding mice. The data are expressed as mean ± SEM, $*p < 0.05$.

compared to those of the SCD groups. Interestingly, after 16 weeks of HFD feeding, the iRhom2 KO mice, but not the WT mice, exhibited a smaller body weight gain than the WT groups (Figure 2A). Body composition examination also revealed a lower fat mass in the HFD-fed iRhom2 KO mice than in the HFD-fed WT mice, although the lean mass in the HFD-fed iRhom2 KO mice did not differ markedly from the HFD-WT mice (Figure 2B,C). The HFD-fed iRhom2-deficient and HFD-WT mice did not display significant changes in their food or water intake (Figure 2A—D). Of note, previous studies demonstrated that prolonged HFD intake promotes insulin resistance and glucose intolerance [23—25]. When aspects of obesity were investigated, phenotypes of obesity and lipid accumulation in the liver were significantly demonstrated in the HFD-fed WT mice compared with those in the HFD-treated iRhom2 KO mice (Figure 2D), suggesting that iRhom2 deficiency may relieve HFD-induced obesity. In particular, the time-course records (every four weeks) of the blood glucose and insulin in the HFD-fed iRhom2 KO mice were lower than those in the WT mice, and there were significant differences in the area under the curve (AUC) and HOMA-IR index (Figure 2E—G). Accordingly, we further examined the changes in insulin-resistance signaling in the HFD-fed KO and WT mice. Following continuous HFD feeding for 16 weeks, the metabolism- and insulin-associated IRS-AKT-GSK3β and FOXO1-PEPCK pathways were investigated via western blotting. The experiments revealed decreased PEPCK levels and enhanced phosphorylation of $IRS1^{Y608}$, AKT, GSK3β, and FOXO1 in the iWAT and eWAT samples of the iRhom2 KO mice compared with those in the corresponding controls (Figure 2E). The iRhom2 KO mice consistently demonstrated restored insulin sensitivity and improved glucose tolerance compared with the WT mice as evidenced by the glucose-tolerance test (GTT) and insulin-tolerance test (ITT) (Figure 2F,G). Of note, the HFD-fed iRhom2 KO mice exhibited downregulated fat mass and blood glucose but no significant differences in bone mineral density compared to the corresponding control mice (Fig. S2H). The adipose and liver tissues were further subjected to hematoxylin and eosin (H&E) staining to visualize the impaired status of the tissues (Figure S2I). Specifically, the iRhom2 KO tissues demonstrated a slight difference in liver morphology in the HFD-fed mice and a markedly restrained fatty liver morphology compared with the HFD-fed WT mice. Histological analysis also indicated that the white adipocyte size and cell numbers were markedly reduced in the HFD-fed iRhom2 KO mice compared with those in the WT mice (Figure S2J—L). An immunohistochemical assay of the F4/80 expression in the adipose tissues revealed that iWAT and eWAT exhibited lower F4/80-positive cell activity in the iRhom2 KO mice compared with the WT mice fed HFD fodder, suggesting that iRhom2 expression in fat tissues may contribute to HFD-triggered macrophage activation and adipose inflammation infiltration (Figure S2M).

3.3. Changes in iRhom2 activity coupled with a high-fat diet triggered adipose inflammation and dyslipidemia

Given the close relationships among obesity, insulin resistance, inflammation, and abnormal lipid metabolism, we next investigated the influence of iRhom2 on lipid metabolism and adipose inflammation. The HFD-fed iRhom2 KO mice demonstrated a lower activation of TNF-α/NF-κB signaling in iWAT than the HFD-fed WT mice (Figure 3A). Moreover, qPCR analysis of the iWAT samples from the mice that underwent HFD treatment revealed that the mRNA expression levels of the genes associated with cholesterol synthesis (sterol regulatory element-binding protein 1c [SREBP-1c] and 3-hydroxy-3-methyl-glutaryl-coenzyme A reductase [HMGCR]), fatty acid uptake (fatty acid transport protein 1 [FATP1], fatty acid-binding protein [FABP1] and

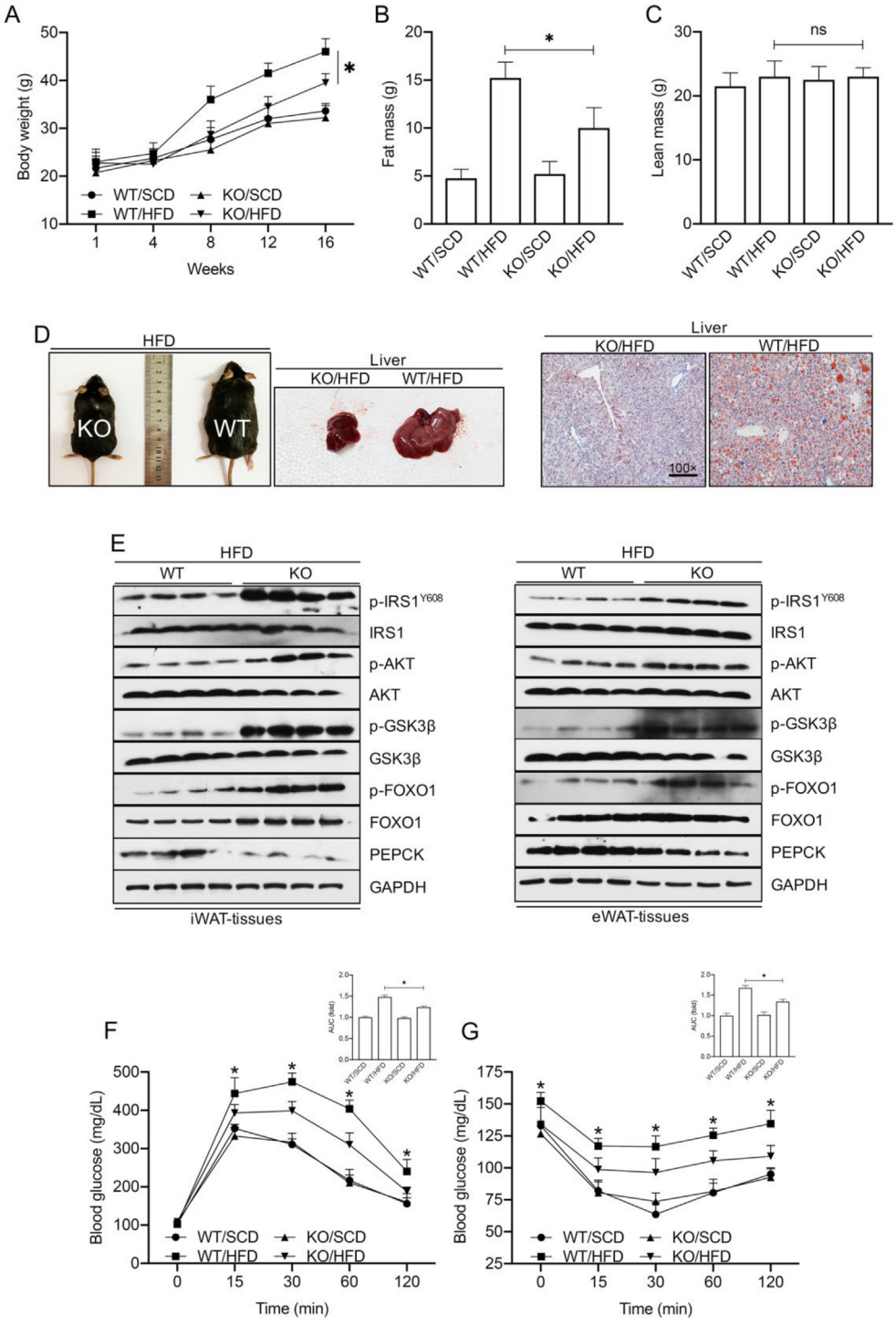

Figure 2: iRhom2 deficiency exhibits decreased fat mass and insulin resistance. (A) Body weight of male C57BL/6N WT and iRhom2 KO mice during SCD and HFD feeding, $n = 15$. (B) Fat mass and (C) lean mass in male C57BL/6N WT and iRhom2 KO mice with SCD and HFD feeding, $n = 15$. (D) Representative photos of HFD-fed WT mice, iRhom2 KO mice, appearance of the liver, and Oil Red O stained hepatic sections (100× magnification). (E) Representative immunoblot bands of the levels of insulin resistance-associated signaling expression including phosphorylated IRS1^{Y608}, AKT, GSK3β, FOXO1, and PEPCK in iWAT and eWAT from HFD-fed WT and iRhom2 KO mice. (F) Glucose tolerance test and (G) insulin tolerance test of HFD or SCD-fed WT and iRhom2 KO mice, $n = 15$. The data are expressed as mean ± SEM. *$p < 0.05$ vs iRhom2 KO/HFD. (For interpretation of the references to colour in this figure legend, the reader is referred to the Web version of this article.)

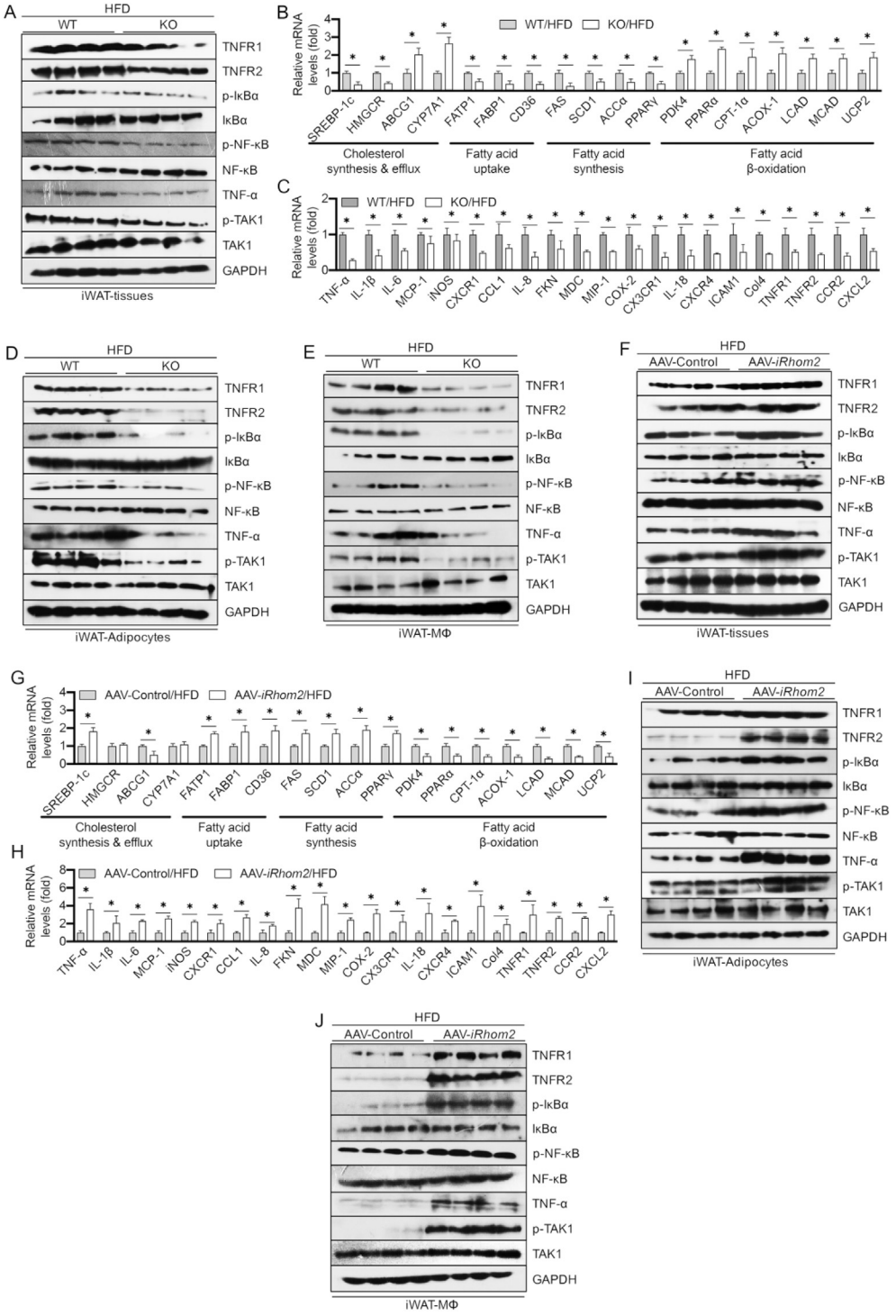

Figure 3: iRhom2 contributes to adipose inflammatory responses in obese mice. (A) Representative immunoblot bands of the expression of inflammation-related signaling including TNFR1/2, phosphorylated IκBα, NF-κB, TAK1, and TNF-α. qPCR analysis detection of the mRNA expression of the genes responsible for (B) lipid metabolism and (C) inflammatory cytokines and chemokines in HFD-fed WT and iRhom2 mice, $n = 6$. Representative western blotting bands of the expression of inflammatory signaling in (D) adipocytes and (E) F4/80 ± macrophages isolated from iWAT of HFD-fed WT and iRhom2 mice. (F) Western blotting analysis of inflammatory signaling in iWAT of HFD-fed AAV-iRhom2 overactivated and corresponding mice. mRNA expression of the genes responsible for (G) lipid metabolism and (H) inflammatory cytokines and chemokines in HFD-fed AAV control and AAV-iRhom2 overactivated mice, $n = 6$. Western blotting of the expression of inflammation indicators in (I) adipocytes and (J) F4/80 ± macrophages from iWAT of AAV control and AAV-iRhom2 overactivated mice. The data are expressed as mean ± SEM, $^*p < 0.05$.

CD36), and fatty acid synthesis (fatty acid synthase [FAS], stearoyl-CoA desaturase [SCD1], acetyl CoA carboxylase α [ACCα], and peroxisome proliferator-activated receptor γ [PPARγ]) were markedly inhibited, whereas the mRNA expression levels of the genes involved in cholesterol efflux (ATP-binding cassette sub-family G member 1 [ABCG1] and cholesterol 7α-hydroxylase [CYP7A1]) and fatty acid β oxidation (pyruvate dehydrogenase kinase 4 [PDK4], peroxisome proliferator-activated receptor α [PPARα], carnitine palmitoyltransferase 1α [CPT-1α], acyl-coenzyme A oxidase 1, [ACOX-1], long-chain acyl-CoA dehydrogenases [LCAD], medium-chain acyl-CoA dehydrogenase [MCAD], and uncoupling protein 2 [UCP2]) were dramatically upregulated in the iRhom2 KO mice relative to those in the corresponding WT mice (Figure 3B). Reduced activation of the inflammation-associated mRNA levels in the iWAT of the HFD-fed iRhom2 KO mice, including TNF-α, IL-1β, IL-6, MCP-1, iNOS, CXCR1, CCL1, IL-8, FKN, MDC, MIP-1, COX-2, CX3CR1, IL-18, CXCR4, ICAM1, Col4, TNFR1/R2, CCR2, and CXCL2 (Figure 3C) and downregulated serum levels of inflammatory chemokines and cytokines (Figure S3A) such as TNF-α, IL-1β, IL-6, MCP-1, CCL1, IL-18, IL-17, IL-2, IL-10, IL-5, MIP-2, MIP-3β, MCP-3, PCT, HMGB1, MDC, GCP-2, CX3CL1, CXCL10, and CXCL12 were significantly and consistently demonstrated compared with those in the HFD-fed WT mice. Of note, lower TNF-α/NF-κB signaling activation in the adipocytes and MΦs isolated from the iWAT was also determined as evidenced by western blotting (Figure 3D,E). Similarly, examination of indicators (Figsure S4A—E) in the eWAT displayed a nearly consistent pattern of expression with those of inflammatory and lipid-metabolic indicators relative to the iWAT in the HFD-fed iRhom2 mice as indicated by qPCR and western blotting. These results demonstrated that iRhom2 may directly contribute to HFD-induced adipose inflammation and dyslipidemia partly by enhancing adipocyte inflammation and macrophage activation. To better understand this, the mice were treated with adeno-associated virus (AAV) packaged with iRhom2 vectors to generate iRhom2 overexpression mice. As expected, after long-term HFD intake, an excess activation of iRhom2 in the mice promoted adipose inflammation, dyslipidemia development (Figure 3F—J), and increased serum inflammatory cytokine and chemokine production (Figure S3B). The changes in these indicators in the eWAT were next examined via qPCR and Western blotting. Collectively, these results significantly suggest that iRhom2 is a key linker involved in HFD-stimulated adipose inflammation and dyslipidemia.

3.4. Myeloid cell-specific iRhom2 knockout reduces high-fat diet-induced adipose inflammation and dyslipidemia

The data in this study demonstrate the role of iRhom2 in HFD-induced adipose inflammation and macrophage activation. We next explored the role of iRhom2 in macrophages in adipose inflammation using bone marrow transplantation (BMT), a widely used method of changing the gene expression of macrophages [26,27]. Lethally irradiated WT mice were transplanted with bone marrow cells isolated from the iRhom2 KO and/or WT mice to generate KOBM→WT mice. After an HFD treatment for 16 weeks, the KOBM→WT/HFD mice, in which iRhom2 was deleted only in the myeloid cells, and the WTBM→WT/HFD mice, in which iRhom2 was integrated in all of the cells, had similar body weights and compositions (Figure 4A,B). Interestingly, the KOBM→WT/HFD mice exhibited improved insulin sensitivity and restored glucose tolerance than the WTBM→WT/HFD mice as evidenced by the GTT and ITT and the AUC index (Figure 4C,D). Accordingly, when the expressions of insulin resistance-associated indicators of the iWAT were examined, the KOBM→WT/HFD mice showed a reduced severity of insulin-resistance signaling, including reduced p-IRS^{Y608}, p-AKT, p-GSK3β, p-FOXO1, and PEPCK levels than the WTBM→WT/HFD mice (Figure 4E). When macrophage activation of the iWAT was detected, the KOBM→WT/HFD mice also demonstrated reduced TNF-α/NF-κB signaling activation as indicated by Western blotting (Figure 4F). Furthermore, as indicated by changes in the mRNA expression levels of lipid metabolism and adipose inflammation, the KOBM→WT/HFD mice exhibited downregulated severity of dyslipidemia-related indicators compared with the WTBM→WT/HFD mice (Figure 4G). The WTBM→WT/HFD mice also expressed dramatically more inflammatory cytokines and chemokines, in terms of mRNA levels, than the KOBM→WT/HFD mice (Figure 4H). These results indicate that iRhom2 deficiency, specifically in myeloid cells (MΦs), reduces the severity of HFD-induced obesity and insulin resistance.

3.5. Myeloid cell-specific iRhom2 expression increases high-fat diet-induced adipose inflammation and dyslipidemia

To better understand the role of iRhom2 in the MΦs in the regulation of the pathogenesis of obesity, we next transplanted bone marrow cells isolated from the WT and/or iRhom2 KO mice into lethally irradiated iRhom2 KO mice to create WTBM→KO mice. After an HFD treatment for 16 weeks, the WTBM→KO/HFD mice, in which iRhom2 was integrated only in the myeloid cells, and the KOBM→KO/HFD mice, in which iRhom2 was impaired in all cells, exhibited no significant differences in body weights or body compositions (Figure S5A and B). However, the HFD-treated WTBM→KO/HFD mice demonstrated increased glucose tolerance and insulin resistance than the HFD-fed KOBM→KO/HFD mice (Figure S5C and D) as determined by the GTT and ITT and the AUC index. We subsequently investigated the altered expressions of insulin resistance-associated indicators of iWAT in the HFD-fed mice. The WTBM→KO/HFD mice displayed upregulated insulin-resistance signaling, including upregulation of p-IRS^{Y608}, p-AKT, p-GSK3β, p-FOXO1, and PEPCK levels, compared to the KOBM→KO/HFD mice (Figure S5E). When the statuses of inflammatory responses in the iWAT were examined, the WTBM→KO/HFD mice also exhibited significant increases in TNF-α/NF-κB signaling activation compared with the corresponding control mice as indicated by western blotting (Figure S5F). Additionally, as determined by changes in the mRNA expression levels of components of lipid metabolism and adipose inflammation, the WTBM→KO/HFD mice demonstrated increased dyslipidemia-related indicators than the KOBM→KO/HFD mice (Figure S5G). The WTBM→KO/HFD mice consistently produced markedly more inflammatory cytokines and chemokines in terms of their mRNA levels than the KOBM→KO/HFD mice (Figure S5H). Taken together, the results presented in Figure 4 and Figure S5 significantly demonstrate a destructive role of iRhom2 in macrophages during HFD-triggered adipose inflammation and dyslipidemia.

4. DISCUSSION

The prevalence of obesity has increased dramatically in most industrialized countries over the past few decades. Obesity is a systemic disease that unleashes a prolonged low level of inflammation in insulin-targeted organs, including the muscle, fat, and liver. This inflammation results in an overloaded production of a series of cytokines and chemokines that trigger systemic insulin resistance [28—31]. Many prior studies demonstrated that obesity increases the likelihood of many diseases, particularly cardiovascular and cerebrovascular diseases, such as type II diabetes mellitus, nonalcoholic fatty liver disease, obstructive sleep apnea, atherosclerosis, certain types of cancer, and osteoarthritis [32—36]. Mechanistically, chronic

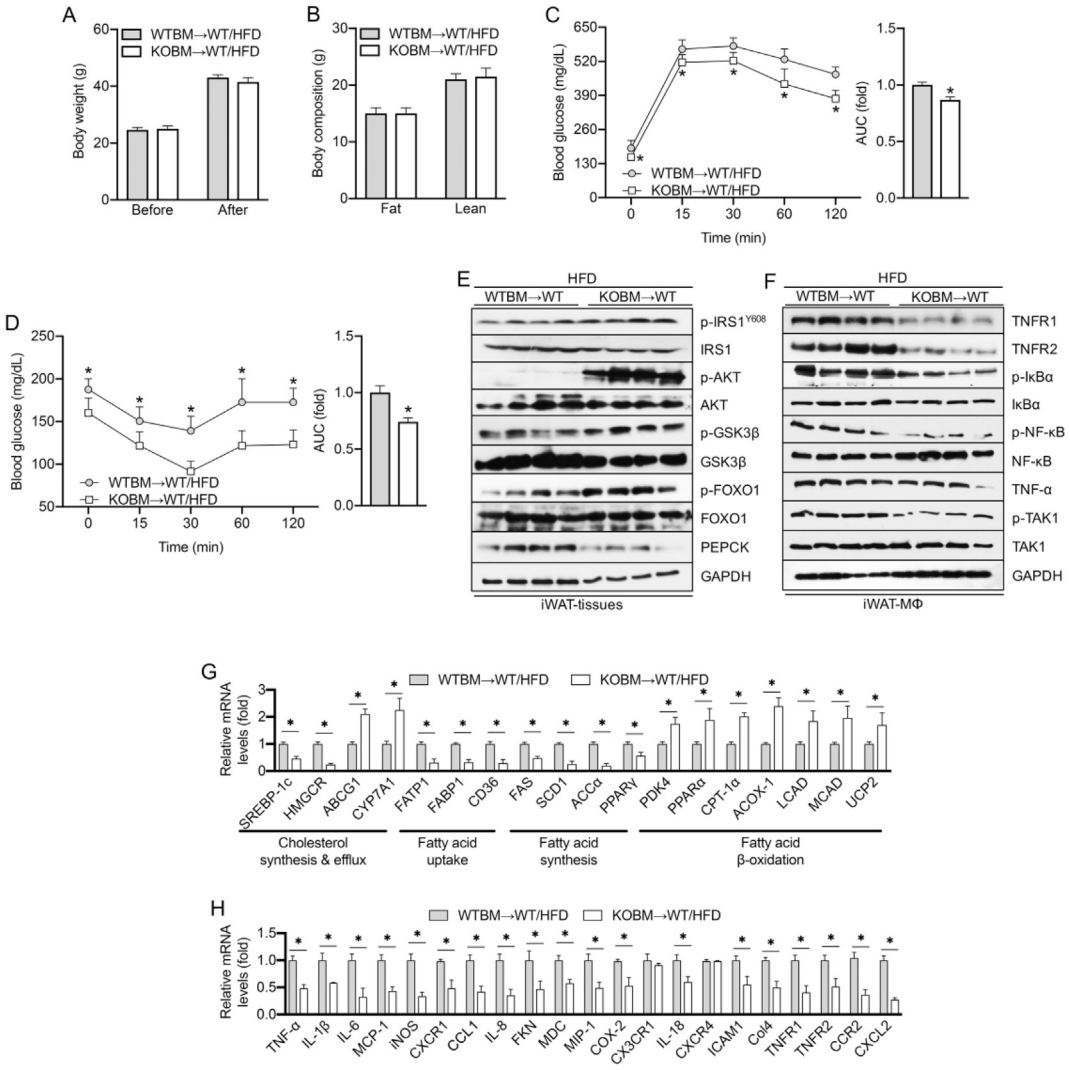

Figure 4: Myeloid cell-specific iRhom2 deletion downregulates insulin resistance and inflammation in obese mice. (A) Body weight was examined before and after the feeding period, $n = 15$. (B) Body composition, $n = 10$. (C) Glucose and (D) insulin tolerance test, $n = 15$. Western blotting bands of the expression of (E) insulin signaling from iWAT and (F) inflammation signaling of F4/80+ macrophages in iWAT. mRNA expression of the genes responsible for (G) lipid metabolism and (H) inflammatory cytokines and chemokines in HFD-fed WTBM→WT/HFD and KOBM→WT/HFD mice, $n = 6$. The data are expressed as mean ± SEM, $^*p < 0.05$.

inflammation infiltration plays a critical role in obesity-stimulated metabolic disorder and various metabolism-associated diseases [2]. Unfortunately, the molecular mechanisms by which obesity leads to insulin resistance, systemic inflammation, and metabolic diseases are still not fully understood. Interestingly, iRhom2, an inactive member of the rhomboid intramembrane-proteinase family of serine proteases, has been elucidated to be a key regulator of innate immunity [15–17,37,38]. In the present study, a series of *in vivo* experiments determined that adipose iRhom2 is involved in insulin resistance and inflammatory responses. Using different mouse models of obesity, we further confirmed that iRhom2 plays a significantly accelerative role in obesity-induced sustained systemic metabolic disorders. Previous studies suggested that iRhom2 is a crucial pathogenic mediator of inflammatory responses and is required for the production of TNF-α secretion in immune cells [13,16]. iRhom2 found in myeloid cells (MΦs) is required for overnutrition stress to stimulate or promote obesity and its associated metabolic disorder aspects in mice. In essence, overactivation by obesity dramatically elevates macrophage inflammatory levels that then upregulate adipocyte insulin resistance and further aggravate adipose inflammatory responses and chemotactic macrophage activation. We demonstrated that sustained iRhom2 is an adverse regulator in obesity via promoting insulin resistance and macrophage activation associated with pro-inflammatory responses of fat tissues.

Our prior studies found that mice with a sustained HFD exhibited significant adipose inflammation and nonalcoholic fatty liver disease-like pathological phenotypes compared with corresponding control mice [39,40]. This current mouse model of obesity revealed upregulation of the phosphorylation levels of NF-κB, TNF-α, and TNFR1/2 in fat tissues, adipocytes, SVFs, and macrophages, demonstrating elevated activation events downstream of iRhom2. We also observed consistently elevated phosphorylated NF-κB in *db/db* mice (a model of genetic obesity) accompanied by upregulated adipose inflammation that included overactivated downstream iRhom2 events. These results revealed a crosslink in iRhom2 signaling and obesity. We also confirmed the mechanism of elevated iRhom2 activity with obesity-

associated metabolic disorder by investigating the indicators of metabolic syndrome. We revealed a disadvantageous effect of iRhom2 in obesity-induced insulin resistance and adipose inflammation. We posit that the loss of iRhom2 may alleviate metabolic disorders caused by obesity. As evidence, the iRhom2-deficient mice were protected against HFD-induced obesity and associated body weight gain, insulin resistance, abnormal lipid homeostasis, and increased adipocyte size and numbers compared with the control groups. For adipose inflammation pathogenesis, macrophage infiltration significantly contributes to the development and process of metabolic dysfunction. Predictably, iRhom2 deficiency restrained F4/80-positive macrophage activation in the adipose tissues. Importantly, iRhom2 knockout promoted whole-body glucose and lipid metabolism balance in HFD-induced obesity. Hence, we sought to confirm whether the overexpression of iRhom2 accelerated obesity-triggered insulin resistance and dyslipidemia. Specifically, iRhom2 overexpression in mice was constructed using an adenovirus-associated virus 8 (AAV8) delivery system. In contrast to the iRhom2 knockout mice, overactivation of iRhom2 resulted in increased downstream TNFR1/2 signaling, which further phosphorylated and activated NF-κB, promoting the expression of a series of inflammatory cytokines and chemokines in the fat tissue, adipocytes, and F4/80-positive macrophages, such as TNF-α, IL-1β, IL-6, MCP-1, CCL1, IL-18, IL-17, IL-2, IL-10, IL-5, MIP-2, MIP-3β, MCP-3, PCT, HMGB1, MDC, GCP-2, CX3CL1, CXCL10, and CXCL12. iRhom2 overactivation in the HFD-fed mice markedly and consistently maintained lipid homeostasis disequilibria-associated gene expression, including increased cholesterol synthesis, fatty acid uptake and synthesis, and decreased fatty acid efflux and β oxidation.

Previous studies indicated that iRhom2 plays a key role in regulating the maturation of TNF-α convertase (ADAM17), which manages the shedding of TNF-α by trafficking with ADAM17 and pro-inflammatory activity *in vivo* [12,16]. However, apart from in the macrophages, where iRhom2 is expressed at high levels, TNF-α-associated inflammatory response in other cell types does not depend on iRhom2. As previously reported [21], in response to stimulation, the expression of iRhom2 in macrophages significantly upregulated and promoted TNF-α production by trafficking the TNF-α-converting enzyme (ADAM17). iRhom2 is the only control switch for inflammatory activation of immune cells via production of TNF-α. However, this happens only in immune cells. TNF-α in general somatic cells does not rely on iRhom2 signaling. Adipocytes play a key role in the regulation of adipose inflammation (mostly induced by macrophage activation) and insulin resistance. iRhom2-regulated pro-inflammatory macrophage activation-triggered inflammatory infiltration mainly results in adipose inflammation and insulin resistance. To elucidate the essential role of iRhom2 in macrophage-activation-related insulin resistance and metabolic dysfunction, we obtained additional findings from BMT mice to understand the sustained harmful effects of iRhom2 in myeloid cells in the progression and pathogenesis of obesity. In the functional-deficit experiments, the BMT mice in which iRhom2 was deleted, specifically in the myeloid cells, exhibited energetic glucose tolerance and reduced insulin resistance compared with the mice in which iRhom2 was uninjured in all of the cells. Conversely, in functional acquisition experiments, the BMT mice that had uninjured iRhom2 specifically in their myeloid cells showed increased glucose intolerance, insulin resistance, and severity of HFD-induced obesity than mice in which iRhom2 was impaired in all of the cells. The comparative studies indicated that myeloid cell (macrophage)-specific iRhom2 influences the production of cytokines in HFD-induced adipose inflammation and metabolic dysfunction. Of note, the HFD-stimulated obesity phenotype in the BMT mice in which iRhom2 was impaired only in the myeloid cells demonstrated less adipose inflammation and abnormal levels of lipid-metabolism-related indicators than mice in which iRhom2 was intact in all of the cells. In contrast, the HFD-stimulated obesity phenotype in the BMT mice in which iRhom2 was not destructive only in the myeloid cells exhibited a higher expression of adipose inflammation and lipid metabolism disorder-related indicators than mice in which iRhom2 was deleted in all of the cells. Of note, there were no significant differences in the body weights and compositions of the corresponding BMT animals in the comparative experiment. The data indicated that iRhom2-regualated macrophage pro-inflammatory activation partly contributed to weight loss, obesity-associated adipose inflammation, lipid metabolism, and insulin resistance.

In conclusion, the current study identified a novel effect of iRhom2 on obesity and insulin resistance that relies on the crosslinks and interactions of iRhom2 with obesity-induced macrophage activation,

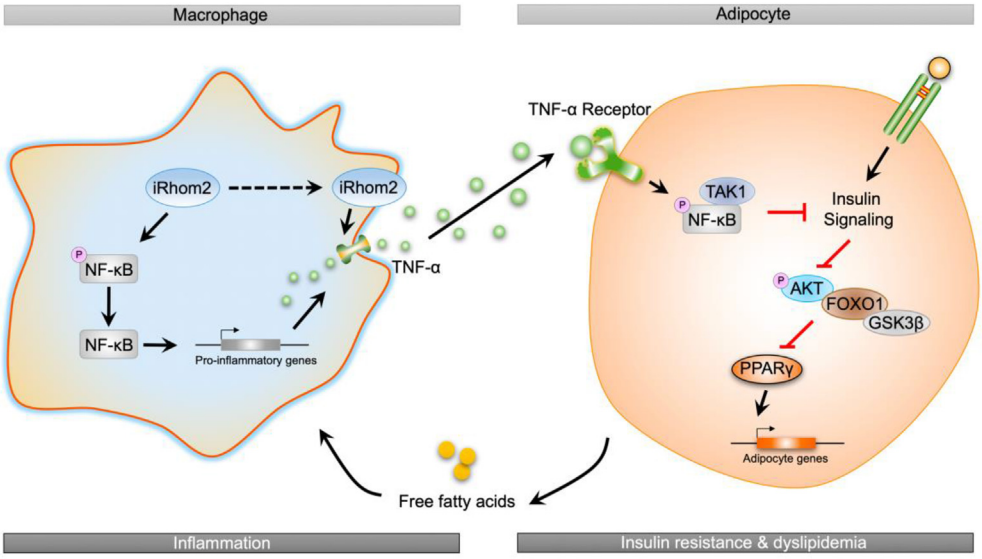

Figure 5: A schematic diagram demonstrating the possible role of iRhom2 in high-fat diet-induced adipose inflammation and insulin resistance.

which enhances TNFR1/2 signaling, downstream TNF-α events, and phosphorylated NF-κB cascades, leading to insulin resistance, adipose inflammation, and dyslipidemia in response to an HFD (Figure 5). We further indicated that the decrease or increase in macrophage-specific iRhom2 expression constitutionally had a deleterious effect on adipose inflammation and insulin resistance, which was confirmed by promoting macrophage pro-inflammatory activation. Therefore, HFD-induced insulin resistance and adipose inflammation phenotype partially depends on iRhom2-regualted macrophage activation. These conclusions potentially and partly provide evidence that iRhom2 may represent a therapeutic target and promising treatment approach for obesity and its associated metabolic diseases.

ACKNOWLEDGMENTS

This study was jointly supported by (1) the National Natural Science Foundation of China (NSFC Grant No.: 81703527); (2) the Chongqing Research Program of Basic Research and Frontier Technology (Grant Nos.: cstc2017jcyjAX0356, cstc2018jcyjA3686, cstc2018jcyjAX0784, cstc2018jcyjA1472, cstc2018jcyjAX0811, cstc2018jcyjA3533, and KJZD-M201801601); (3) the School-Level Research Program of Chongqing University of Education (Grant Nos.: KY201710B and 17GZKP01); (4) Advanced Programs of Post-Doctor of Chongqing (Grant No.: 2017LY39); (5) the Science and Technology Research Program of Chongqing Education Commission of China (Grant Nos.: KJQN201901608, KJQN201901615, and KJ1601402); (6) the Children's Research Institute of the National Center for Schooling Development Program and Chongqing University of Education (Grant No.: CSDP19FSO1108); and (7) the Chongqing Professional Talents Plan for Innovation and Entrepreneurship Demonstration Team (Grant No.: CQCY201903258).

DECLARATION OF COMPETING INTERESTS

Minxuan Xu, Chenxu Ge, Yuting Qin, Deshuai Lou, Qiang Li, Jing Feng, Yekuan Wu, Linfeng Hu, Bochu Wang, and Jun Tan declare that they have no conflicts of interest.

APPENDIX A. SUPPLEMENTARY DATA

Supplementary data to this article can be found online at https://doi.org/10.1016/j.molmet.2020.01.008.

REFERENCES

[1] Heymsfield, S.B., Wadden, T.A., 2017. Mechanisms, pathophysiology, and management of obesity. New England Journal of Medicine 376(3):254—266.
[2] Saltiel, A.R., Olefsky, J.M., 2017. Inflammatory mechanisms linking obesity and metabolic disease. Journal of Clinical Investigation 127(1):1—4.
[3] Reilly, S.M., Saltiel, A.R., 2017. Adapting to obesity with adipose tissue inflammation. Nature Reviews Endocrinology 13(11):633.
[4] Lackey, D.E., Olefsky, J.M., 2016. Regulation of metabolism by the innate immune system. Nature Reviews Endocrinology 12(1):15.
[5] Lee, B.C., Kim, M.S., Pae, M., Yamamoto, Y., Eberlé, D., Shimada, T., et al., 2016. Adipose natural killer cells regulate adipose tissue macrophages to promote insulin resistance in obesity. Cell Metabolism 23(4):685—698.
[6] Dalmas, E., Toubal, A., Alzaid, F., Blazek, K., Eames, H.L., Lebozec, K., et al., 2015. Irf5 deficiency in macrophages promotes beneficial adipose tissue expansion and insulin sensitivity during obesity. Nature Medicine 21(6):610.
[7] Lumeng, C.N., Bodzin, J.L., Saltiel, A.R., 2007. Obesity induces a phenotypic switch in adipose tissue macrophage polarization. Journal of Clinical Investigation 117(1):175—184.
[8] Olefsky, J.M., Glass, C.K., 2010. Macrophages, inflammation, and insulin resistance. Annual Review of Physiology 72:219—246.
[9] Kalupahana, N.S., Moustaid-Moussa, N., Claycombe, K.J., 2012. Immunity as a link between obesity and insulin resistance. Molecular Aspects of Medicine 33(1):26—34.
[10] de Heredia, F.P., Gómez-Martínez, S., Marcos, A., 2012. Obesity, inflammation and the immune system. Proceedings of the Nutrition Society 71(2):332—338.
[11] Shimobayashi, M., Albert, V., Woelnerhanssen, B., Frei, I.C., Weissenberger, D., Meyer-Gerspach, A.C., et al., 2018. Insulin resistance causes inflammation in adipose tissue. Journal of Clinical Investigation 128(4).
[12] Adrain, C., Zettl, M., Christova, Y., Taylor, N., Freeman, M., 2012. Tumor necrosis factor signaling requires iRhom2 to promote trafficking and activation of TACE. Science 335(6065):225—228.
[13] Siggs, O.M., Xiao, N., Wang, Y., Shi, H., Tomisato, W., Li, X., et al., 2012. iRhom2 is required for the secretion of mouse TNFα. Blood 119(24):5769—5771.
[14] Luo, W.W., Li, S., Li, C., Lian, H., Yang, Q., Zhong, B., et al., 2016. iRhom2 is essential for innate immunity to DNA viruses by mediating trafficking and stability of the adaptor STING. Nature Immunology 17(9):1057.
[15] McIlwain, D.R., Lang, P.A., Maretzky, T., Hamada, K., Ohishi, K., Maney, S.K., et al., 2012. iRhom2 regulation of TACE controls TNF-mediated protection against Listeria and responses to LPS. Science 335(6065):229—232.
[16] Maretzky, T., McIlwain, D.R., Issuree, P.D.A., Li, X., Malapeira, J., Amin, S., et al., 2013. iRhom2 controls the substrate selectivity of stimulated ADAM17-dependent ectodomain shedding. Proceedings of the National Academy of Sciences 110(28):11433—11438.
[17] Chenxu, G., Minxuan, X., Yuting, Q., Tingting, G., Jinxiao, L., Mingxing, W., et al., 2018. iRhom2 loss alleviates renal injury in long-term PM2. 5-exposed mice by suppression of inflammation and oxidative stress. Redox biology 19:147—157.
[18] Issuree, P.D.A., Maretzky, T., McIlwain, D.R., Monette, S., Qing, X., Lang, P.A., et al., 2013. iRHOM2 is a critical pathogenic mediator of inflammatory arthritis. Journal of Clinical Investigation 123(2):928—932.
[19] Lichtenthaler, S.F., 2013. iRHOM2 takes control of rheumatoid arthritis. Journal of Clinical Investigation 123(2).
[20] Xu, M.X., Ge, C.X., Qin, Y.T., Gu, T.T., Lou, D.S., Li, Q., et al., 2018. Multi-combination approach suppresses listeria monocytogenes-induced septicemia-associated acute hepatic failure: the role of iRhom2 signaling. Advanced Healthcare Materials 7(17):1800427.
[21] Christova, Y., Adrain, C., Bambrough, P., Ibrahim, A., Freeman, M., 2013. Mammalian iRhoms have distinct physiological functions including an essential role in TACE regulation. EMBO Reports 14(10):884—890.
[22] Menghini, R., Fiorentino, L., Casagrande, V., Lauro, R., Federici, M., 2013. The role of ADAM17 in metabolic inflammation. Atherosclerosis 228(1):12—17.
[23] Schweiger, M., Romauch, M., Schreiber, R., Grabner, G.F., Hütter, S., Kotzbeck, P., et al., 2017. Pharmacological inhibition of adipose triglyceride lipase corrects high-fat diet-induced insulin resistance and hepatosteatosis in mice. Nature Communications 8:14859.
[24] Huypens, P., Sass, S., Wu, M., Dyckhoff, D., Tschöp, M., Theis, F., et al., 2016. Epigenetic germline inheritance of diet-induced obesity and insulin resistance. Nature Genetics 48(5):497.
[25] Vial, G., Chauvin, M.A., Bendridi, N., Durand, A., Meugnier, E., Madec, A.M., et al., 2015. Imeglimin normalizes glucose tolerance and insulin sensitivity and improves mitochondrial function in liver of a high-fat, high-sucrose diet mice model. Diabetes 64(6):2254—2264.
[26] Xu, H., Li, H., Woo, S.L., Kim, S.M., Shende, V.R., Neuendorff, N., et al., 2014. Myeloid cell-specific disruption of Period1 and Period2 exacerbates diet-induced inflammation and insulin resistance. Journal of Biological Chemistry 289(23):16374—16388.
[27] Lan, T., Li, C., Yang, G., Sun, Y., Zhuang, L., Ou, Y., et al., 2018. Sphingosine kinase 1 promotes liver fibrosis by preventing miR-19b-3p-mediated inhibition of CCR2. Hepatology 68(3):1070—1086.

[28] Ellulu, M.S., Patimah, I., Khaza'ai, H., Rahmat, A., Abed, Y., 2017. Obesity and inflammation: the linking mechanism and the complications. Archives of Medical Science: AMS 13(4):851.

[29] Wu, H., Ballantyne, C.M., 2017. Skeletal muscle inflammation and insulin resistance in obesity. Journal of Clinical Investigation 127(1):43–54.

[30] Baidal, J.A.W., Lavine, J.E., 2016. The intersection of nonalcoholic fatty liver disease and obesity. Science Translational Medicine 8(323), 323rv1-323rv1.

[31] Nishimoto, S., Fukuda, D., Higashikuni, Y., Tanaka, K., Hirata, Y., Murata, C., et al., 2016. Obesity-induced DNA released from adipocytes stimulates chronic adipose tissue inflammation and insulin resistance. Science advances 2(3): e1501332.

[32] James, W.P.T., Caterson, I.D., Coutinho, W., Finer, N., Van Gaal, L.F., Maggioni, A.P., et al., 2010. Effect of sibutramine on cardiovascular outcomes in overweight and obese subjects. New England Journal of Medicine 363(10): 905–917.

[33] Mozaffarian, D., 2016. Dietary and policy priorities for cardiovascular disease, diabetes, and obesity: a comprehensive review. Circulation 133(2): 187–225.

[34] Miller, J.D., Aronis, K.N., Chrispin, J., Patil, K.D., Marine, J.E., Martin, S.S., et al., 2015. Obesity, exercise, obstructive sleep apnea, and modifiable atherosclerotic cardiovascular disease risk factors in atrial fibrillation. Journal of the American College of Cardiology 66(25):2899–2906.

[35] Berenbaum, F., Eymard, F., Houard, X., 2013. Osteoarthritis, inflammation and obesity. Current Opinion in Rheumatology 25(1):114–118.

[36] Marengo, A., Rosso, C., Bugianesi, E., 2016. Liver cancer: connections with obesity, fatty liver, and cirrhosis. Annual Review of Medicine 67:103–117.

[37] Khokha, R., Murthy, A., Weiss, A., 2013. Metalloproteinases and their natural inhibitors in inflammation and immunity. Nature Reviews Immunology 13(9): 649.

[38] Luo, W.W., Li, S., Li, C., Zheng, Z.Q., Cao, P., Tong, Z., et al., 2017. iRhom2 is essential for innate immunity to RNA virus by antagonizing ER-and mitochondria-associated degradation of VISA. PLoS Pathogens 13(11):e1006693.

[39] Chenxu, G., Minxuan, X., Yuting, Q., Tingting, G., Jing, F., Jinxiao, L., et al., 2019. Loss of RIP3 initiates annihilation of high-fat diet initialized nonalcoholic hepatosteatosis: a mechanism involving Toll-like receptor 4 and oxidative stress. Free Radical Biology and Medicine 134:23–41.

[40] Xu, M., Ge, C.X., Qin, Y.T., Gu, T., Lv, J., Wang, S., et al., 2019. Activated TNF-α/RIPK3 signaling is involved in prolonged high fat diet-stimulated hepatic inflammation and lipid accumulation: inhibition by dietary fisetin intervention. Food & function. https://doi.org/10.1039/C8F001615A.

[41] Liu, M., Bai, J., He, S., Villarreal, R., Hu, D., Zhang, C., et al., 2014. Grb10 promotes lipolysis and thermogenesis by phosphorylation-dependent feedback inhibition of mTORC1. Cell Metabolism 19(6):967–980.

[42] Hussaarts, L., García-Tardón, N., van Beek, L., Heemskerk, M.M., Haeberlein, S., van der Zon, G.C., et al., 2015. Chronic helminth infection and helminth-derived egg antigens promote adipose tissue M2 macrophages and improve insulin sensitivity in obese mice. The FASEB Journal 29(7):3027–3039.

[43] Fernyhough, M.E., Vierck, J.L., Hausman, G.J., Mir, P.S., Okine, E.K., Dodson, M.V., 2004. Primary adipocyte culture: adipocyte purification methods may lead to a New understanding of adipose tissue growth and development. Cytotechnology 46(2–3):163–172.

